

## Strained $InGaAs/InAlAs$ High Electron Mobility Transistors

Pallab Bhattacharya

*Solid State Electronics Laboratory, Department of Electrical Engineering & Computer Science  
University of Michigan, Ann Arbor, Michigan 48109-2122, USA*

### ABSTRACT

The direct current (dc) and microwave performance of  $InP$ -based  $In_xGa_{1-x}As/In_{0.52}Al_{0.48}As$  strained high electron mobility transistors are described. Its design is based on theoretical and experimental studies including low- and high-field transport characterisation of heterostructures with different strains. Mobilities as high as 13,900; 74,000 and 134,000  $cm^2/Vs$  are measured at 300, 77 and 4.2 K in a heterostructure with the value of  $x$  being 0.65. Shubnikov-de Haas measurements indicate that the change in the effective mass with increasing  $In$  is not significant in  $n$ -HEMTs and is not responsible for the enhancement in mobilities. We believe that the improvement results from reduced alloy scattering, reduced intersub-band scattering, and reduced impurity scattering, all of which result from a higher conduction-band offset and increased carrier confinement in the two-dimensional electron gas. The high field electron velocities have been measured in these samples using pulsed current-voltage and pulsed Hall measurements. A monotonic increase in velocities is observed both at 300 and 77 K with an increase of  $In$  content in the channel. Velocities of  $1.55 \times 10^7$  and  $1.87 \times 10^7$   $cm/s$  are measured at 300 and 77 K, respectively, in a  $In_{0.65}Ga_{0.35}As/In_{0.52}Al_{0.48}As$  modulation-doped heterostructure. In 1.4  $\mu m$  gate HEMTs, the maximum intrinsic dc transconductor is 700  $mS/mm$  when  $x = 0.65$ . The highest values of  $f_T$  and  $f_{max}$  are 45 GHz and 60 GHz respectively. These figures clearly indicate their superiority over identical lattice-matched devices, primarily resulting from increased first sub-band confinement in the pseudomorphic quantum well channel. It is expected that by reducing gate lengths to submicron dimensions and making some growth-related changes in heterostructure design, the best millimetre wave solid-state low-noise amplifiers and oscillators can be realised.

## 1. INTRODUCTION

Since the first demonstration of high carrier mobilities achievable in modulation-doped heterojunctions<sup>1,2</sup>, these structures have attracted great interest for their intrinsic physical properties and their potential application to high speed devices. The possible device applications of two-dimensional electron gas (2-DEG) systems in field-effect transistors (FETs) have formed the focus of intense activity in many laboratories over the past decade<sup>3</sup>. Transistor performances achieved with *GaAs/AlGaAs* lattice-matched heterojunctions to date significantly exceed the best results obtainable with more conventional devices in terms of speed, low noise performance, and power-delay products<sup>4-12</sup>. It is, therefore, likely that the high electron mobility transistors, (HEMT) or MODFET as they are often called, will attain wide industrial importance for millimetre wave communications, supercomputers, and instrumentation.

*GaAs/AlGaAs* HEMT devices exhibit excellent direct current (dc) and radio frequency (RF) performance at room temperature, but degrade at 77 K and lower temperatures, where the device might prove to be useful for space and extra-terrestrial applications. The commonly observed 'collapse' of the  $I$ - $V$  characteristics<sup>13,14</sup> in these devices results from the presence of dominant electron traps, called  $D$ - $X$  centres<sup>15</sup> in the  $Al_xGa_{1-x}As$  layer for  $x \geq 0.24$ . Some technique to circumvent the problem such as pulse-doping in the *AlGaAs* region, or replacing it with a *GaAs/AlGaAs* superlattice, whose wells are only doped, have resulted in mixed success.  $In_{0.53}Ga_{0.47}As/In_{0.52}Al_{0.48}As$  HEMTs lattice-matched to *InP* have shown excellent performance at 300 K due to lower electron effective masses, higher electron mobilities and velocities, and a higher band offset  $\Delta E_c$  at the hetero-junction. For example,  $g_{m(ext)} = 400$  mS/mm and  $f_T = 35$  GHz are measured for 1  $\mu$ m gate devices<sup>16,17</sup>. For 0.2 and 0.1  $\mu$ m gate lengths, devices of 50  $\mu$ m width exhibit extrinsic transconductances of 800 and 1080 mS/mm, respectively<sup>18</sup>. External  $f_T$  of 170 GHz was obtained from a  $0.1 \times 200$   $\mu$ m<sup>2</sup> device. A minimum noise figure of 0.8 dB and associated gain of 8.7 dB were obtained from a single-stage amplifier at V band<sup>18</sup>. These represent world-record performances from transistors. However, at lower temperatures, the expected benefits in this heterostructure are largely curtailed due to the mobilities being limited by alloy scattering in *InGaAs*<sup>19</sup>. There is, therefore, a need to use heterostructure systems where the above mentioned problems are minimised or completely removed, in addition to providing other advantages. Strained heterostructure systems have, therefore, emerged as attractive materials for the design and fabrication of high performance HEMTs.

There are two types of strained heterostructures being used for HEMT fabrication. The first is with substrates with a large mismatch. Examples are *GaAs/AlGaAs* on *Si* with a 4 per cent misfit, or  $In_{0.5}Ga_{0.5}As/In_{0.5}Al_{0.5}As$  on *GaAs* with a 3.5 per cent misfit. The advantages here result from a possible increase in band offset and slight tailoring of effective mass and is driven by the needs of optoelectronic integration. In the second class of strained HEMTs the 2-DEG is formed in a pseudomorphic channel, and therefore, in addition to tailoring  $\Delta E_c$ , there is a possibility to drastically change the effective masses and carrier scattering rates through an alteration of the bandstructure. This effect is more pronounced in the valence band, where, for example, with the application of biaxial tensile strain, the light-hole band is raised in energy above the heavy-hole band. The subsequent expected lowering of the hole effective masses would be extremely useful for the design of *p*-HEMTs and complementary logic.

Although good performance has been reported in pseudomorphic  $In_xGa_{1-x}As/Al_{0.15}Ga_{0.85}As$  HEMTs<sup>20-24</sup>, further improvements can only be obtained either by increasing

the *In* content ( $x$ ) in *InGaAs*, or the *Al* content in *AlGaAs*. The former will increase alloy scattering, while the latter will result in the presence of the *D-X* centre in *AlGaAs*, with the associated detrimental effects. It is clear, therefore, that to get uniformly high performance at 300 and 77 K, one needs to consider the  $In_{0.53+x}Ga_{0.47-x}As/InAlAs/InP$  system, or low bandgap binary compounds, so that the effects of alloy scattering are reduced, at the same time, reaping the benefits of biaxial strain. In this paper the material properties and HEMT performance in  $In_{0.53+x}Ga_{0.47-x}As/InAlAs$  heterostructures on *InP* substrates will be briefly discussed.

## 2. GROWTH OF STRAINED LAYERS BY MOLECULAR BEAM EPITAXY

### 2.1 Growth Modes

In lattice-matched systems, the general nature of growth in molecular beam epitaxy (MBE) is fairly well understood. The growth front during MBE can be described as being in between two extreme growth modes: (a) a layer-by-layer growth mode where the growth front essentially consists of at most two exposed (cation) monolayers and even though atoms impinge randomly from the vapour phase, they move rapidly on the exposed surface and attach themselves at step edges; and (b) a three-dimensional growth mode where the impinging atoms have essentially no surface kinetics and the surface is rough due to the intrinsic statistical fluctuations. These growth modes can be readily observed by *in situ* reflection high-energy electron diffraction (RHEED). In the case of strained epitaxy, in to considerations arising from second neighbour bond strengths, one has also to with the strain energy. Theoretical and experimental studies<sup>25</sup> have been carried to understand the initial stages of growth of *InGaAs* on *GaAs*. Thermodynamic ; show that, as strain increases, the free-energy minimum surface of the is not atomically flat, but three-dimensional in form (Fig. 1). Since by altering

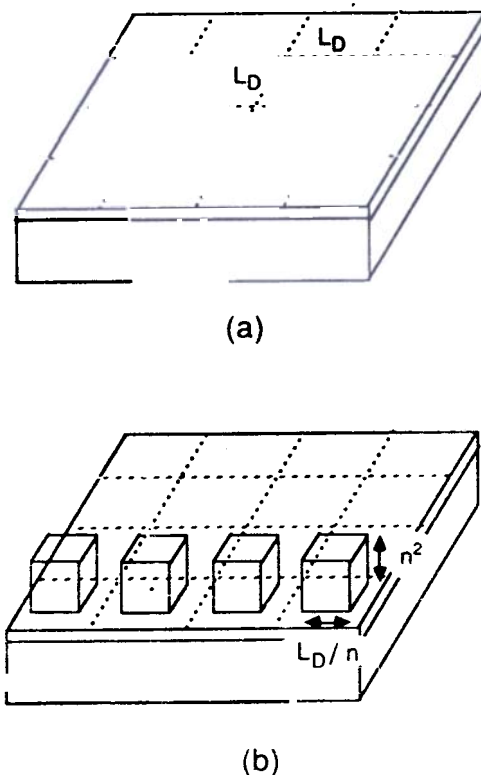


Figure 1. A schematic showing the two cases where (a) a monolayer of the lattice mismatched epilayer is arranged in an atomically flat monolayer under coherent strain, and (b) the atoms from 3-D islands with bases of side  $L_D/n$  and height  $n^2$ .

growth conditions the strained epilayer can be grown near equilibrium or far from equilibrium, the effect of strain on growth modes can be studied. *In situ* RHEED studies were carried out to study the growth modes and surface lattice spacing before the onset of dislocations. It was found that the surface lattice constant does not change abruptly from that of the substrate to that of the epilayer at the critical thickness, but changes monotonically. These observations are consistent with simple thermodynamic considerations. The height of the islands can be expressed as

$$n^3 = 2(W_1/W_2) (R_0/d_c) \quad (1)$$

where  $W_1$  and  $W_2$  are first and second neighbour bond strengths respectively,  $R_0$  is the surface lattice constant and  $d_c$  is the critical thickness. In other words, misfit dislocations are produced at the substrate-epilayer interface for film thicknesses exceeding  $d_c$ . Equation (1) suggests that if  $d_c < 20$  monolayers (i.e., strain  $> 2$  per cent) the strained epilayer will minimise its energy by forming three-dimensional islands. For small misfits, although island formation may not be very pronounced, it is expected and experimentally observed, that the growth front attains a certain degree of roughness. A rough heterointerface in HEMTs can be extremely detrimental to the performance characteristics.

## 2.2 Interfacial Characteristics of Strained Heterostructures

The structural properties of the heterointerface, at which the 2-DEG is formed in a HEMT, are crucial for achieving state-of-art performance. A rough surface can give rise to enhanced interface roughness scattering, which degrades the transport and high frequency performance of the HEMT. An excellent technique to probe the quality of the heterointerface is to analyse the low temperature excitonic linewidths in quantum wells made of the same materials. Such studies<sup>26</sup> have shown that the excitonic linewidth of a 100 Å ternary well is primarily determined by alloy broadening and interface roughness.

We have investigated<sup>27</sup> the molecular beam epitaxial growth and optical properties of  $In_xGa_{1-x}As/GaAs$  ( $0.07 \leq x \leq 0.20$ ) single quantum wells and multiple quantum well structures. Photoluminescence and absorption measurements were made to characterise the various structures. Low temperature excitonic linewidths as small as 1.2 to 2.4 meV have been obtained in 80 to 120 Å  $In_xGa_{1-x}As/GaAs$  ( $0.07 \leq x \leq 0.20$ ) single and multiple quantum wells up to total thicknesses of 2.0 μm (Fig. 2). The Stokes shift in these samples is ~ 1 to 2 meV. This result is independent of the absence or presence of an intermediate composition buffer layer and indicates that the latter does not influence the optical properties of strained multiquantum wells. The growth kinetics and growth modes are more important factors in this respect. These experiments with the growth kinetics have given us valuable information regarding the techniques to be adapted for strained-layer MBE. In our laboratories, we use similar techniques for the growth of  $InGaAs/InAlAs/InP$  strained heterostructures.

Another striking result that has recently been obtained by us in the fact that when growing strained-layer superlattices (SLS), the total thickness that can be achieved without the generation of misfit dislocations (for the average SLS composition) is many times larger than that in a single layer of the same average composition. Cross-sectional transmission electron micrographs (TEM) and optical absorption studies clearly indicates the absence of propagating misfit dislocations and that the SLS is in a metastable state. This is an extremely important experimental observation, and recent calculations by Van der Merwe *et al.*<sup>28</sup> predict a similar behaviour.

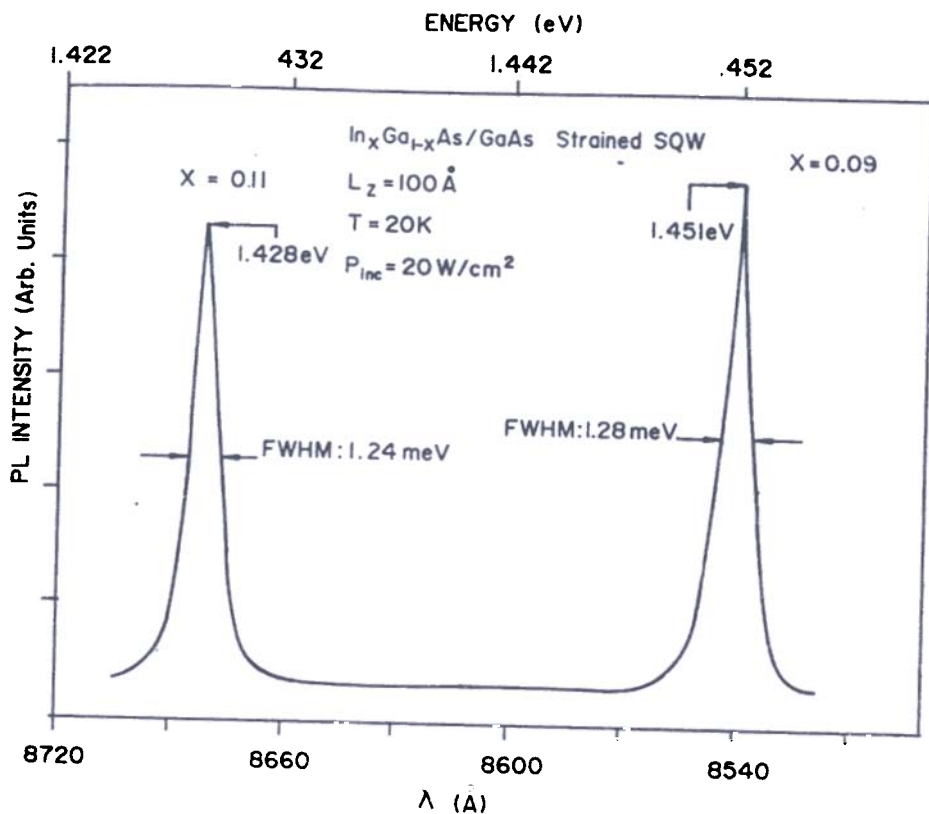


Figure 2. Low temperature photoluminescence spectra of  $In_xGa_{1-x}As/GaAs$  strained single quantum well with  $L_z = 100 \text{ \AA}$  obtained with  $5145 \text{ \AA}$  excitation. The well with the higher indium content was grown first, followed by well with smaller  $x$ . The barrier in between the wells is  $\sim 0.45 \text{ \mu m}$ .

### 3. TRANSPORT PROPERTIES

#### 3.1 HEMT Design and MBE Growth

The schematic diagram of the structures and corresponding band diagrams are shown in Fig. 3. The modulation-doped (MD) heterostructures consist of a  $0.4 \text{ \mu m}$  undoped  $In_{0.52}Al_{0.48}As$  buffer, a  $400 \text{ \AA}$  undoped  $In_{0.53}Al_{0.47}As$  layer, a  $150 \text{ \AA}$  undoped  $In_xGa_{1-x}As$  channel, a  $100 \text{ \AA}$  undoped  $In_{0.52}Al_{0.48}As$  spacer layer,  $200 \text{ \AA}$  Si-doped ( $3 \times 10^{18} \text{ cm}^{-3}$ )  $In_{0.52}Al_{0.48}As$  layer, a  $300 \text{ \AA}$  undoped  $In_{0.52}Al_{0.48}As$ , and finally a  $200 \text{ \AA}$  Si-doped ( $3 \times 10^{18} \text{ cm}^{-3}$ )  $In_{0.53}Al_{0.47}As$  for ohmic contacts. Three types of samples were grown with different  $In$  mole fractions in the  $In_xGa_{1-x}As$  channel region:  $x = 0.53, 0.60,$  and  $0.65$ . Growth interruptions for 1 min were used at the interface before the  $In_xGa_{1-x}As$  channel to accomplish higher  $In$  mole fractions by changing the  $Ga$  fluxes.

#### 3.2 Low and High Field Mobilities and Velocities

The dependence of the electron transport properties on the  $In$  mole fraction in the channel was investigated<sup>29</sup> by low and high field transport measurements. Cloverleaf and Hall bar geometries were used for low field Hall measurements by the Van der Pauw technique and Shubnikov-de Haas measurements respectively. The high field transport properties were determined from pulsed current-voltage measurements on planar H-shaped devices at 300 K, and pulsed Hall measurements at 300 and 77 K on hall bars. The room temperature electron velocities were computed from the currents measured during the pulsed current-voltage temperatures while the low temperature (77 K) electron

n	InGaAs	3 E18	200A
n	InAlAs	3E18	
i	In(x)Ga(1-x)As	150A	
i	InGaAs	400A	
i	InAlAs	4000A	
	InAlAs/InGaAs	S.L.	
S.I.		100 )	

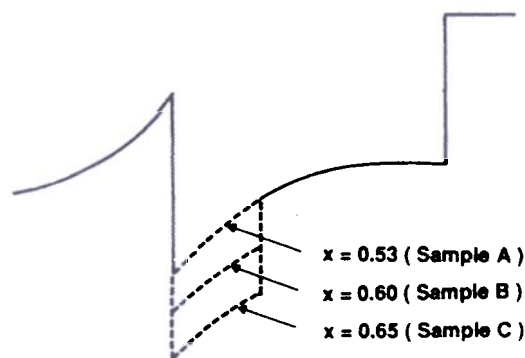


Figure 3. Schematic of pseudomorphic modulation-doped heterostructures and corresponding band diagrams.

velocities were calculated from the mobility-field characteristics determined by the pulsed Hall measurements.

Temperature-dependent Hall mobilities measured in the various samples are shown in Fig. 4. At low temperatures, the mobilities increase slowly, indicating the two-dimensional characteristics of carriers in the channel. Mobility and carrier concentration data at 300 and

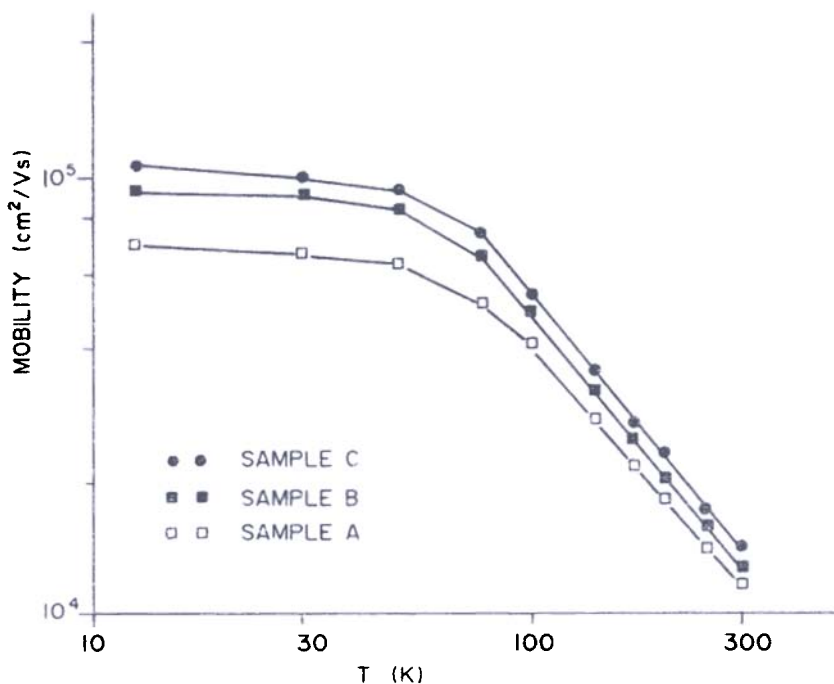


Figure 4. Temperature dependent Hall mobilities measured in samples A, B and C.

77 K for the three samples are summarised in Table 1. As can be seen, the increase in the sheet carrier concentration with the addition of excess *In* is modest. With 65 per cent *In* in the channel, a carrier density increase of approximately 10 per cent is obtained with the same doping. The band gap of the  $In_xGa_{1-x}As$  channel material decreases with the increase of *In* mole fraction, leading to an increase in the conduction band discontinuity and better confinement. The latter leads to the observed increase in 2-DEG carrier concentration.

Table 1. Measured Hall data from  $In_xGa_{1-x}As/In_{0.52}Al_{0.48}As$  heterostructure

Sample	Channel composition	Mobility ( $cm^2/Vs$ )		2-DEG Density ( $10^{12}cm^{-2}$ )	
		(300 K)	(77 K)	(300 K)	(77 K)
A	0.53	11,500	50,100	1.65	1.60
B	0.60	12,300	65,200	1.79	1.74
C	0.65	13,900	74,000	1.82	1.79

According to the Shubnikov-de Haas data given in Table 2, most of the carriers (more than 95 per cent of total carriers) are residing in the first sub-band in samples with 60 per cent and 65 per cent *In* channels. The difference in energy between  $E_0$  and  $E_1$  also significantly increases in samples B and C. Therefore, it is not difficult to expect reduced intersub-band scattering with increase of *In* mole fraction in the channel material. Therefore, the increase in carrier confinement in the lowest sub-band and effects associated with it, namely, reduced remote impurity scattering and reduced intersub-band scattering, play the most important role in the enhancement of low field mobilities which is experimentally observed in the strained channel heterostructures. Alloy scattering limited mobility is also increased, by a factor of 10 per cent, by the increase of the *In* content.

Table 2. Transport data obtained from Hall and Shubnikov-de Haas measurements

Sample(x)	Hall data at 4.2 K		$m^*/m_0$	$N_0^a$	$N_1^b$	$E_1 - E_0^c$
	$\mu_H(cm^2/Vs)$	$n_H(10^{12}cm^{-2})$				
A(0.53)	67,900	1.46	$0.046 \pm 0.002$	1.12	0.26	43.2
B(0.60)	95,000	1.65	$0.046 \pm 0.002$	1.53	0.04 <sup>d</sup>	76.1
C(0.65)	134,000	1.65	$0.046 \pm 0.002$	1.65	0.04 <sup>d</sup>	84.6

- a) Lowest sub-band occupation at 4.2 K determined from Shubnikov-de Haas measurements.  
 b) Occupation in first excited sub-band at 4.2 K.  
 c) Energy separation between ground state and first excited state in the 2-DEG.  
 d) These values are approximate.

The velocity-field characteristics of electrons obtained from pulsed current-voltage measurements at room temperature are shown in Fig. 5. The electron velocity was calculated from the output current density recorded on a sampling oscilloscope. Measurements were made up to fields of 2.25 kV/cm and electron velocities were observed to increase monotonically in all three samples. Maximum velocities of 1.35, 1.45, and  $1.55 \times 10^7$  cm/s were calculated at  $E = 2.25$  kV/cm for samples A, B and C respectively. It is to be noted that no velocity saturation was observed at room temperature in any of the samples. The velocities at 77 K, also shown in Fig. 5, were obtained from measured mobility-field characteristics by using the relation

$$v(E) = \mu(E) E \quad (2)$$

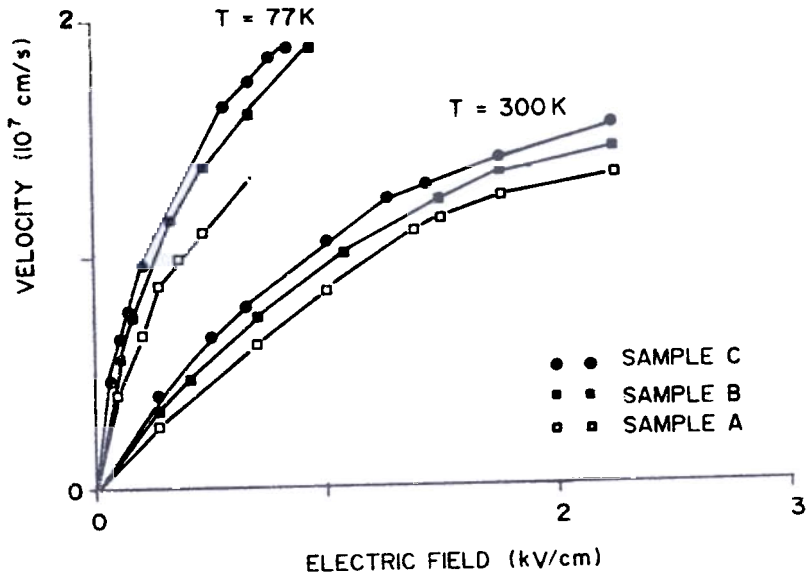


Figure 5. Velocity-field characteristics obtained from pulsed current-voltage measurements and pulsed Hall measurements at 300 K and 77 K respectively.

It is clear that electron velocities are increased with an increase in  $In$  content in the channel in the entire range of electric fields scanned during the measurements. It is also expected that velocity saturations will occur at higher fields, but these cannot be accurately measured due to the onset of instabilities. The enhancement of electron velocity is thought to be the main contributor to the superior device performance observed in samples  $B$  and  $C$  compared to that in sample  $A$ .

### 3.3 Carrier Effective Masses

As stated earlier, changes of in-plane effective masses are expected in pseudomorphic HEMTs through a change in the bandstructure caused by the biaxial strain. From Table 2 it

## 4. DC AND MICROWAVE DEVICE CHARACTERISTICS

Because of the drastic improvement in the transport properties of  $In_xGa_{1-x}As$

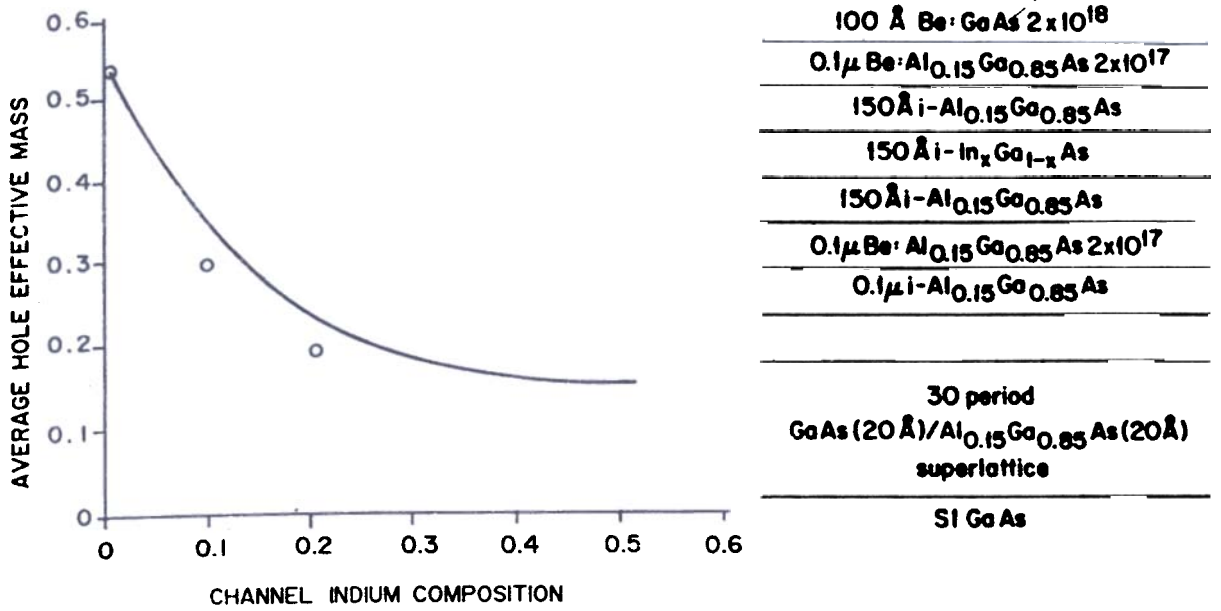


Figure 6. Measured hole effective masses in  $p$ -type  $In_xGa_{1-x}As/GaAs$  modulation-doped heterostructures schematically shown in the inset. The line represents theoretically calculated values<sup>31</sup>.

$In_{0.52}Al_{0.48}As$   $n$ -HEMTs with increase of strain, we have studied<sup>32,33</sup> the dc and microwave properties of 1 μm gate  $In_{0.65}Ga_{0.35}As/In_{0.52}Al_{0.48}As$  modulation-doped devices. The device structure, grown by MBE, is described in Section 3.1. It was found that an improvement of performance can be expected if the thickness of the strained channel is set to 150 Å. This thickness favour (a) the device mobility, since a large number of carriers concentrate in the strained region, and (b) the output resistance and transconductance by pronounced band splitting and therefore good first sub-band confinement.

The 1.4 μm gate FETs were made with a  $In_{0.65}Ga_{0.35}As/In_{0.52}Al_{0.48}As$  heterostructure by standard photolithography and lift-off techniques.  $Ge/Au/Ni/Ti/Au$  (700/1400/500/200/700 Å) ohmic contacts were formed after isolation mesas were defined and followed by  $Ti$  (500 Å)/ $Au$  (3000 Å) gate formation. Finally,  $Ti$  (1000 Å)/ $Au$  (1 μm) were evaporated for integrated microstrip lines as required for microwave characterisations.

Figure 7 shows the room temperature drain current  $I_d$ , versus voltage  $V_d$ , of a  $1.4 \times 75$

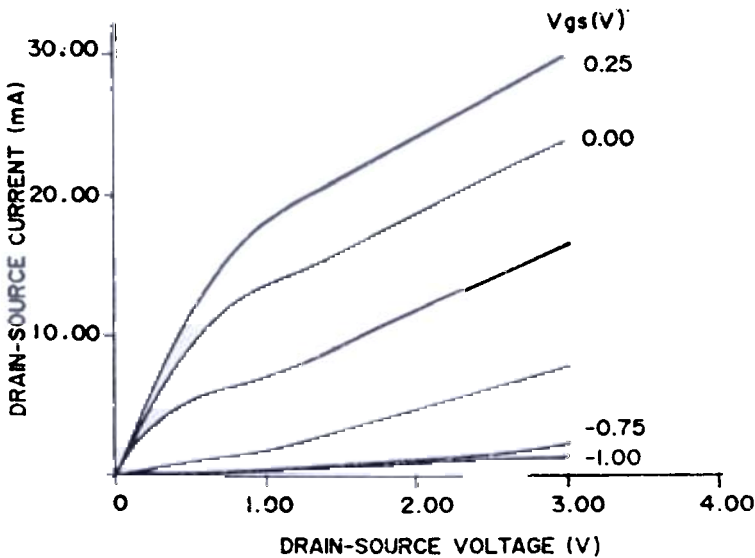


Figure 7. Drain current-voltage characteristics of a  $In_{0.65}Ga_{0.35}As/In_{0.52}Al_{0.48}As$  HEMT with 1.4 μm gate length at 300 K.

$\mu\text{m}^2$  gate HEMT with a 65 per cent *In* channel. The maximum current density of the device is in excess of 500 mA/mm and the dc output conductance is of the order of 5 mS. The peak extrinsic transconductance of this device is 520 mS/mm. The parasitic source access resistance  $R_s$  was evaluated by measuring the total channel resistance as a function of gate length for different patterns under various gate bias conditions. An accurate value of  $R_s$  can be determined in this way ( $R_s = 6.0 \Omega$  for the 75  $\mu\text{m}$  gate-width HEMT). By accounting for this parasitic, the intrinsic transconductance  $g_{m0}$  was evaluated to be 700 mS/mm.

In *GaAs/InAlAs* HEMTs reported up to now have a high output conductance ( $G_{ds}$ ). This high  $G_{ds}$  values are the primary cause of power gain limitation in such devices. For the 150 Å channel design,  $G_{ds}$  varied from 31 to 33 and 39 mS/mm by increasing the *In* from 53 per cent to 60 per cent and 65 per cent. In spite of the better carrier-confinement with strain, the devices show an increase of output conductance which may be attributed to their higher drift velocity and therefore enhanced probability of carrier injection to the buffer. A similar tendency with strain has also been observed for the 100 Å channel designs, supporting the argument of  $G_{ds}$  degradation by enhanced carrier-injection. The overall  $G_{ds}$  values were, however, smaller (9, 16 and 22 mS/mm respectively), due to the better carrier-confinement in thin channels.

Microwave characterisation of the device at different bias conditions (varied  $V_{gs}$  and  $V_{ds}$ ) were performed with a HP8510 network-analyser by CASCADE probing from 0.5 to 26.5 GHz. Their equivalent circuit elements were then extracted by *S*-parameter-fitting. Best results were obtained with the 65 per cent *In* sample. An intrinsic  $f_T$  as high as 45 GHz was obtained. This is believed to be the highest  $f_T$  ever reported for any FET of this gate length. The corresponding unilateral  $f_T$  ( $f_T = g_{m0}/2\pi C_{gs}$ ) was calculated to be 56 GHz. The maximum stable gain at 10 GHz is 12.3 dB and the maximum available gain at 18 GHz is 7.5 dB. The  $f_{max}$  was estimated from the equivalent circuit elements to be 58.9 GHz. The effect of the  $G_{ds}$  is also demonstrated by the fact that, although the 53 per cent and 60 per cent *In*-devices have a lower  $f_T$  of 18 and 37 GHz, their  $f_{max}$  was as high as 78.6 and 59.2 GHz, due to their smaller  $G_{ds}$ .

## 5. SUBMICRON DEVICES WITH HIGHER PSEUDOMORPHIC STRAIN

The results quoted in the previous section clearly demonstrate the potential of the pseudomorphic devices. By reducing gate lengths to 0.25  $\mu\text{m}$  and less, it is anticipated that  $f_T$  and  $f_{max}$  will exceed 150 GHz and 200 GHz, respectively. Such work is in progress in our laboratories and in many others around the world.

It is also important to probe the possibilities of increasing the *In* content in the  $\text{In}_x\text{Ga}_{1-x}\text{As}$  channel beyond  $x = 0.65$ . We have done this and find that for the device structure used here, the mobilities and velocities are actually degraded for  $x > 0.65$ . It is not difficult to understand this, considering the three-dimensional island growth mode in MBE for high degrees of strain. Two structures which we are investigating are depicted in Figs. 8(a) and (b). The first is an inverted HEMT in which the 2-DEG interface is not rough. In the second, Fig. 8(b) an *InAlAs* layer with tensile strain is grown first, so that at the active 2-DEG, there is no resultant strain.

## 6. STABILITY OF PSEUDOMORPHIC STRAINED HEMTs

While most of the early device structures in strained layer superlattices were thermodynamically stable against strain relief, device optimization frequently leads to

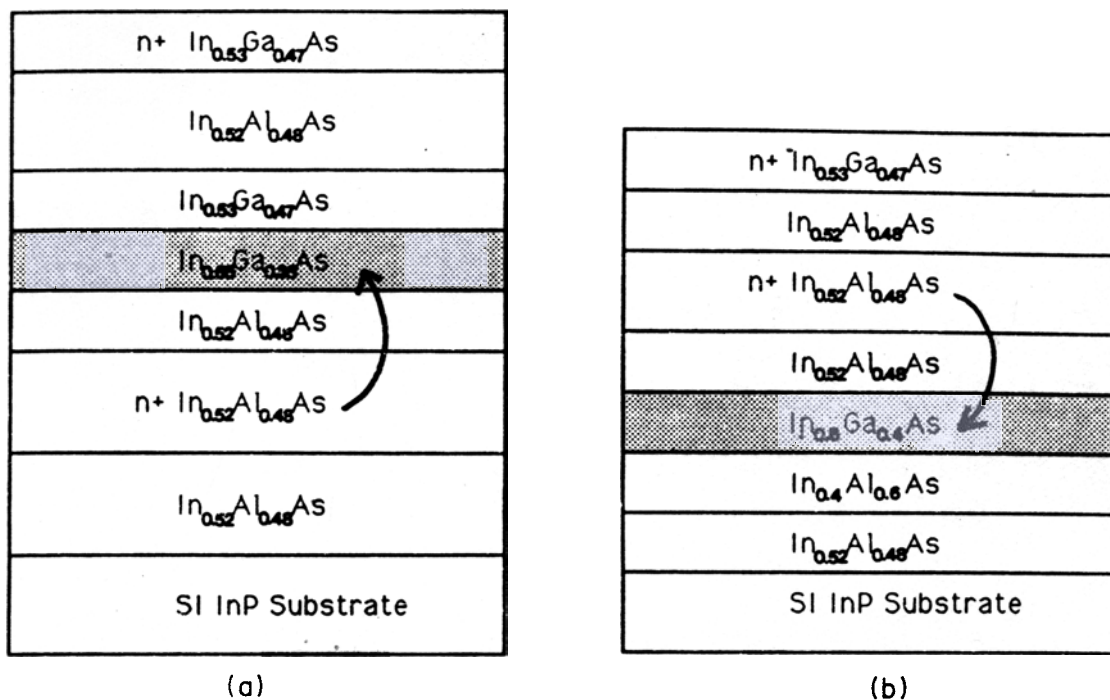


Figure 8. Alternate pseudomorphic *InGaAs/InAlAs* HEMT structures for channels with large *In* content; (a) represents an inverted structure, (b) a layer with tensile strain is incorporated.

metastable structures. These metastable structures have strained layers thicker than the thermodynamically stable critical thickness, yet can be readily grown by a non-equilibrium technique such as MBE, as described in section 2. The as-grown material can exhibit excellent crystalline properties that will not degrade unless sufficient energy—as in thermal annealing—is applied to minimise the free energy by dislocation generation. The implications of metastability and the effects on such structures by high temperature treatments common to device fabrication must therefore be realised. Some work to this end has recently been done by Peercy *et al.*<sup>34</sup>. From their studies, it is concluded that high performance devices can be formed from strained-layer structures. Because the criteria for optimum device performance may conflict with those for structural stability, the best intrinsic device performance is frequently obtained from metastable structures. The performance of FETs fabricated from metastable structures is not expected to degrade with time at any attainable operating temperature; however, special care will be required to integrate them to form complex circuits. In contrast, stable strained-layer structures can withstand the high-temperature processing commonly used for fabrication in compound semiconductor technology.

### 7. $In_{0.5}Ga_{0.5}As/In_{0.5}Al_{0.5}As$ HEMTs ON *GaAs*

In principle, it is possible to grow strain-free mismatched heterostructures with thick buffer layers wherein the strain is relieved with the generation of dislocations. The overriding concerns, in this case, are the surface morphology which is degraded due to the propagating dislocations, and the transport properties, which may be degraded due to interface roughness at the 2-DEG. We have, however, by incorporating a series of heterostructures over which the strain is relieved and the dislocations are bent over, been able to produce modulation-doped  $In_{0.5}Ga_{0.5}As/In_{0.5}Al_{0.5}As$  on *GaAs* with  $\mu_{300K} = 8600$   $cm^2/Vs$  and  $\mu_{10K} = 22,000$   $cm^2/Vs$ . These are the best values produced in such mismatched materials. 1.4  $\mu m$  gate HEMTs made with this system have  $g_m(\text{ext}) \approx 300$   $mS/mm$ , (Fig. 9)

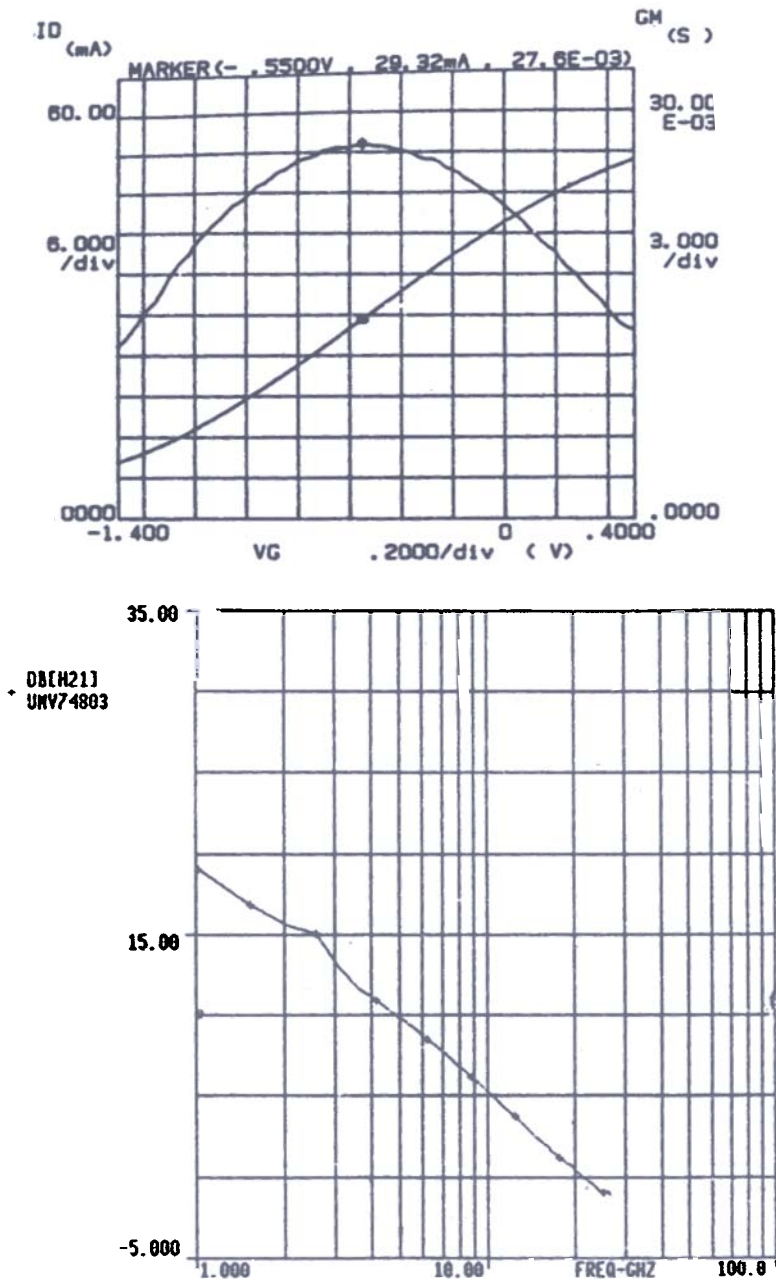


Figure 9. DC and microwave characteristics of 1.4  $\mu\text{m}$  gate  $\text{In}_{0.5}\text{Ga}_{0.5}\text{As}/\text{In}_{0.5}\text{Al}_{0.5}\text{As}$  HEMT-grown on  $\text{GaAs}$  substrates. Upper figure shows the variation of  $g_m$  and  $I_{DS}$  with gate bias and lower figure shows the measured variation of  $h_{21}$  with frequency (a value of  $f_T=21$  GHz is estimated).

$f_T = 21$  GHz, and  $f_{max} = 24$  GHz. These characteristics are extremely encouraging and pave the way for future developments.

### 8. CONCLUSIONS

Recent work on the design and performance of  $\text{InP}$ -based  $\text{In}_x\text{Ga}_{1-x}\text{As}/\text{In}_{0.52}\text{Al}_{0.48}\text{As}$  pseudomorphic HEMTs is described and reviewed. The mobility and velocity improvements with strain are confirmed by Hall, velocity-field, and low temperature Shubnikov-de Haas measurements. It is clear that with modifications in heterostructure design and by incorporating submicron gate dimensions, millimetre wave sources and amplifiers can be made. Reliability issues in these devices, and their relationship to MBE growth, are also briefly discussed.

## ACKNOWLEDGEMENTS

The author would like to thank his colleagues, J. Singh, D. Pavlidis, W-P. Hong, J.E. Oh, M. Jaffe, G.I. Ng, P.R. Berger and J. Pamulapati for their help and useful discussions.

## REFERENCES

1. Dingle, R., Störmer, H.L., Gossard, A.C. & Wiegmann, W., *Applied Phys. Lett.*, **33** (1978), 665.
2. Störmer, H.L., Dingle, R., Gossard, A.C., Wiegmann, W. & Sturge, M.D., *Solid State Commun.*, **29** (1979), 705.
3. Solomon, P.M. & Morkoc, H., *IEEE Trans. on Electron Devices*, **ED-31** (1984), 1015.
4. Mimura, T., Joshin, K., Hiyamizu, S., Hikosaka, K. & Abe, M., *Japan J. Appl. Phys.*, **20** (1981), L598.
5. Delescluse, P., Laviron, M., Chaplart, J., Delagebeaudeuf, D. & Linh, N.T., *Electron. Lett.*, **17** (1981), 342.
6. Lee, C.P., Lee, S.J., Hou, D., Miller, D.L., Anderson, R.J. & Sheng, N.H., *Electron. Lett.*, **20** (1984), 217.
7. Kiehl, R.A., Feuer, M.D., Hendel, R.H., Hwang, J.C.M., Keramidis, V.G., Allyn, C.L. & Dingle, R., *IEEE Electron Dev. Lett.*, **EDL-4** (1983), 377.
8. Takakuwa, H., Kato, Y., Watanabe, S. & Mori, Y., *Electron. Lett.*, **21** (1985), 125.
9. Chao, P.C., Palmateer, S.C., Smith, P.M., Mishra, U.K., Duh, K.H.G. & Hwang, J.C.M., *IEEE Electron. Dev. Lett.*, **EDL-6** (1985), 531.
10. Berenz, J., Nakano, K., Hsu, T-I & Goel, J., *Electron. Lett.*, **21** (1985), 1028.
11. Saunier, P., *IEEE Electron. Dev. Lett.*, **EDL-7** (1986), 503.
12. Christou, A., Varmazis, K. & Hatzopoulos, Z., *Appl. Phys. Lett.*, **50** (1987), 935.
13. Chi, J.Y., Holmstrom, R.P. & Salerno, J.P., *IEEE Electron. Dev. Lett.*, **EDL-5** (1984), 381.
14. Fischer, R., Drummond, T.J., Klem, J., Kopp, W., Henderson, T.S., Perrachione, D. & Morkoc, H., *IEEE Trans. Electron. Devices*, **ED-31** (1984), 1028.
15. Lang, D.V., Logan, R.A. & Jaros, M., *Phys. Rev.*, **B19** (1979), 1015.
16. Seo, K.S., & Bhattacharya, P., *IEEE Trans. Electron Devices*, **ED-34** (1987), 2221.
17. Hong, W-P. & Bhattacharya, P., *IEEE Electron. Dev. Lett.*, **EDL-9** (1988), 352.
18. Mishra, U.K., Brown, A.S., Rosenbaum, S.E., Hooper, C.E., Pierce, M.W., Delaney, M.J., Vaughn, S. & White, K., *IEEE Electron. Dev. Lett.*, **EDL-9** (1988), 647.
19. Basu, P.K. & Nag, B.R., *Appl. Phys. Lett.*, **43** (1983), 689.
20. Zipperian, T.E., & Drummond, T.J., *Electron. Lett.*, **21** (1985), 823.
21. Ketterson, A., Moloney, M., Masselink, W.T., Peng, C.K., Klem, J., Fischer, R., Kopp, W. & Morkoc, H., *IEEE Electron. Dev. Lett.*, **EDL-6** (1985), 628.
22. Henderson, T., Klem, J., Peng, C.K., Gedymin, J.S., Kopp, W. & Morkoc, H., *Appl. Phys. Lett.*, **48** (1986), 1080.
23. Morkoc, H., Henderson, T., Kopp, W. & Peng, C.K., *Electron. Lett.* **22** (1986), 578.

24. Nguyen, L.D., Schaff, W.J., Tasker, P.J., Lepore, A.N., Palmateer, L.F., Foisy, M.C. & Eastman, L.F., *IEEE Trans. Electron. Devices*, ED-35 (1988), 139.
25. Berger, P.R., Bhattacharya, P., Singh, J. & Bajaj, K.K., *Appl. Phys. Lett.*, 53 (1988), 684.
26. Juang, F.Y., Bhattacharya, P., Singh, J. & Nashimoto, Y., *Appl. Phys. Lett.* 48 (1986), 290.
27. Pamulapati, J., Oh, J.E., Debbar, N., & Bhattacharya, P., *J. Appl. Phys.*, to be published.
28. Jesser, W.A., & Van der Merwe, J.H., *J. Appl. Phys.*, 63 (1988), 1928.
29. Hong, W-P., Ng, G.I., Bhattacharya, P.K., Pavlidis, D. & Willing, S., *J. Appl. Phys.*, 64 (1988), 1946.
30. Fritz, I., Schirber, J., Jones, E., Drummond, T.J. & Osbourn, G., *Inst. Phys. Conf. Ser.*, 83 (1986), 233.
31. Jaffe, M., Oh, J., Pamulapati, J., Bhattacharya, P. & Singh, J., Paper presented at the International Symposium on Gallium Arsenide and Related Compounds, Atlanta, 1988.
32. Ng, G.I., Weiss, M., Pavlidis, D., Tutt, M., Bhattacharya, P. & Chen, C. Y., Paper presented at the International Symposium on Gallium Arsenide and Related Compounds, Atlanta, 1988.
33. Ng, G.I., Hong, W-P., Pavlidis, D., Tutt, M., & Bhattacharya, P.K., *IEEE Electron Dev. Lett.*, EDL-9 (1988), 439.
34. Percy, P.S., Dodson, B.W., Tsao, J.Y., Jones, E.D., Myers, D.R., Zipperian, T.E., Dawson, L.R., Biefeld, R.M., Klem, J.F. & Hills, C.R., *IEEE Electron. Dev. Lett.*, EDL-9 (1988), 621.